Mendeleev Communications

Mendeleev Commun., 2025, **35**, 676–680

Slow relaxation of magnetization and luminescence in seven- and six-coordinate Tb^{3+} complexes

Dmitry M. Lyubov,[a,b] Gautier Félix,[c] Aleksey O. Tolpygin,[b] Tatyana V. Mahrova,[b] Yulia V. Nelyubina,[a] Saad Sene,[c] Vladislav M. Korshunov,[d] Ilya V. Taydakov,[a,d] Andrey A. Tyutyunov,[a] Boris Le Guennic,[e] Olivier Cador,[e] Yannick Guari,*[c] Joulia Larionova[c] and Alexander A. Trifonov*[a,b]

[a] *A. N. Nesmeyanov Institute of Organoelement Compounds, Russian Academy of Sciences, 119334 Moscow, Russian Federation. E-mail: trif@iomc.ras.ru*
[b] *G. A. Razuvaev Institute of Organometallic Chemistry, Russian Academy of Sciences, 603950 Nizhnii Novgorod, Russian Federation. E-mail: trif@iomc.ras.ru*
[c] *Charles Gerhardt Montpellier Institute, National Center for Scientific Research, National School of Chemistry of Montpellier, University of Montpellier, 34293 Montpellier, France. E-mail: yannick.guari@umontpellier.fr*
[d] *N. D. Zelinsky Institute of Organic Chemistry, Russian Academy of Sciences, 119991 Moscow, Russian Federation*
[e] *Rennes Institute of Chemical Sciences, National Center for Scientific Research, University of Rennes, 35000 Rennes, France*

DOI: 10.71267/mencom.7860

The synthesis, structures, magnetic and luminescent properties of a new series of mononuclear Tb^{3+} complexes, such as $\{Tb[OCH(CF_3)Ph]_2(THF)_5\}[BPh_4]$, $[Tb(OC_6F_4C_6F_5)_2(THF)_5][BPh_4]$, $\{Tb[OC(CF_3)_2Ph]_2(THF)_4\}[BPh_4]$ and $\{Tb[OC(CF_3)_3]_3(THF)_3\}$, in which fluorinated alkoxide ligands with different steric bulk afford different geometries of the Tb center, are reported. The compound $\{Tb[OCH(CF_3)Ph]_2(THF)_5\}[BPh_4]$, which adopts a pentagonal bipyramidal geometry with an axial O–Tb–O angle of 177.7(5)° and short Tb–O distances, behaves as a field-induced single molecule magnet. All complexes exhibit characteristic Tb^{3+} emission with a relatively long lifetime of up to 1.7 ms.

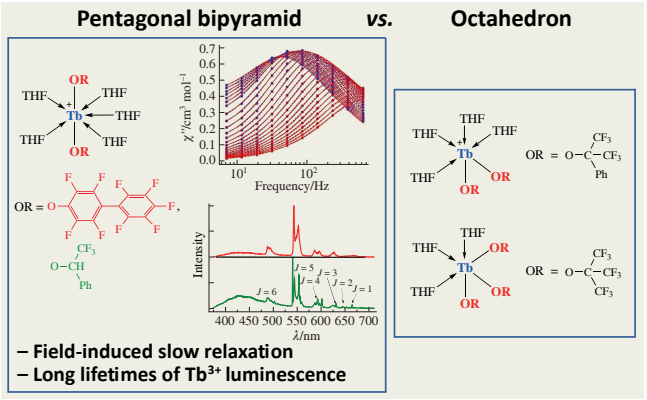

Keywords: terbium, alkoxido ligands, synthesis, structure, pentagonal bipyramidal geometry, octahedral geometry, single molecule magnets, luminescence.

Bifunctional Single-Molecule Magnets (SMMs), which exhibit slow magnetic relaxation combined with optical properties, have garnered significant attention over the past few decades due to their promising applications in cutting-edge technologies.[1–5] These bifunctional materials are particularly compelling because they can independently exhibit both magnetic and optical properties, enabling distinct magnetic and optical readouts crucial for applications such as high-precision sensing and advanced data storage. Furthermore, the interplay of these properties can provide unique functionalities, including light-induced control of magnetic states, luminescence thermometry for precise determination of magnetic transition temperatures and luminescence-based exploration of magnetic barriers, paving the way for innovations in quantum technologies and molecular-scale devices.

The discovery of the first luminescent SMM in 2009[6] gave a powerful impetus to exploring the magnetostructural correlation, with particular emphasis on enhancing magnetic axiality to optimize magnetic relaxation and combining the SMM behavior with luminescence.[7] This has led to the emergence of so-called bifunctional luminescent SMMs, whose optical properties correlate with the energy barriers derived from magnetic characterization, providing insights into the magnetic relaxation mechanisms.[1–4]

Luminescent Tb^{3+}-based SMMs still remain scarce,[8–14] despite the fact that Tb^{3+} coordination compounds typically exhibit bright emissions in the visible spectral window and that Tb^{3+} is the second most widely used lanthanide ion after Dy^{3+} in the development of non-luminescent SMMs. The relatively lower success of Tb^{3+} in contrast to Dy^{3+} in the design of luminescent SMMs could be attributed to its lack of Kramers doublet symmetry, which requires a strictly axial crystal field to achieve magnetic bistability. This makes the selection of ligands to control the lanthanide environment particularly challenging.

The coordination geometry of lanthanide ions is a key factor influencing both their magnetic and luminescent properties. While eight- and nine-coordinate complexes are the most common due to the large size of the lanthanide ions, lower coordination numbers such as six and seven offer opportunities for modulating crystal field effects and anisotropy. In particular, the symmetry and structural distortions associated with such geometries can significantly affect both magnetic relaxation and

luminescence efficiency, as demonstrated by several seven-coordinate complexes, where the specific point group symmetries influence the anisotropy and non-radiative decay pathways.[3,15–20]

In this article, we present a novel family of mononuclear seven- and six-coordinate Tb^{3+} complexes with fluorinated ligands of different steric bulk in combination with coordinated THF ligands. The fluorinated ligands are expected to provide stability and performance to the luminescent SMMs[20–22] by enhancing the structural rigidity through various intermolecular interactions such as hydrogen bonding, π–π···F stacking and halogen bonding. This increased rigidity has been proposed to decrease or suppress vibrational Raman relaxation pathways, thereby optimizing the magnetic relaxation behavior.[23] By suppressing nonradiative deactivation pathways, especially by reducing C–H vibrations, the fluorinated ligands are expected to significantly improve the luminescence performance, making them highly suitable for multifunctional materials. Recently we successfully employed fluorinated ligands to design mononuclear luminescent SMMs based on Dy^{3+} and Er^{3+}. In particular, the obtained compound $[Dy(OCHMeC_6F_5)_2(THF)_5][BPh_4]$ exhibited the characteristic emission of both Dy^{3+} and ligand, as well as the genuine SMM behavior with a high effective energy barrier of 1469 cm^{-1} and a blocking temperature of 22 K.[20] Moreover, the use of such ligands in combination with the Er^{3+} ion led to a series of mono- and dinuclear field-induced SMMs exhibiting Er^{3+} NIR emission, which enabled direct probing of the crystal field splitting in these compounds and its correlation with the magnetic data. Encouraged by these results, we extended our investigations to design a luminescent SMM with the Tb^{3+} ion.

A series of cationic Tb^{3+} complexes $[Tb(L^n)_2(THF)_m][BPh_4]$ **1** [L^1 = $OCH(CF_3)Ph$, m = 5], **2** [L^2 = $OC_6F_4C_6F_5$, m = 5] and **3** [L^3 = $OC(CF_3)_2Ph$, m = 4] were synthesized according to the alkane elimination protocol by the reaction of the tris(*ortho*-dimethylaminobenzyl) complex $Tb(CH_2C_6H_4NMe_2\text{-}o)_3$[24–26] with one equivalent of $[HNEt_3][BPh_4]$ and two equivalents of fluorinated alcohols in THF at ambient temperature (Scheme 1). After recrystallization, the reaction products were obtained by slow diffusion of hexane into THF solution in yields of 75, 79 and 69%, respectively.

However, in the case of the fluorinated alcohol $(CF_3)_3COH$ (L^4H), the same synthesis protocol afforded the neutral tris(alkoxide) complex $[Tb(L^4)_3(THF)_3]$ **4** in 38% yield (see Scheme 1). Most likely, the formation of compound **4** may be associated with the redistribution of ligands of the intermediate cationic complex $[Tb(L^4)_2(THF)_x][BPh_4]$. Targeted synthesis of complex **4** by treating $Tb(CH_2C_6H_4NMe_2\text{-}o)_3$ with three equivalents of $(CF_3)_3COH$ allowed for obtaining it in 76% yield.

X-ray diffraction investigations revealed that compounds **1**–**3** are cationic mononuclear Tb^{3+} complexes that adopt separated ions pair structures, whereas compound **4** is a mononuclear neutral compound based on Tb^{3+} tris(alkoxide).†

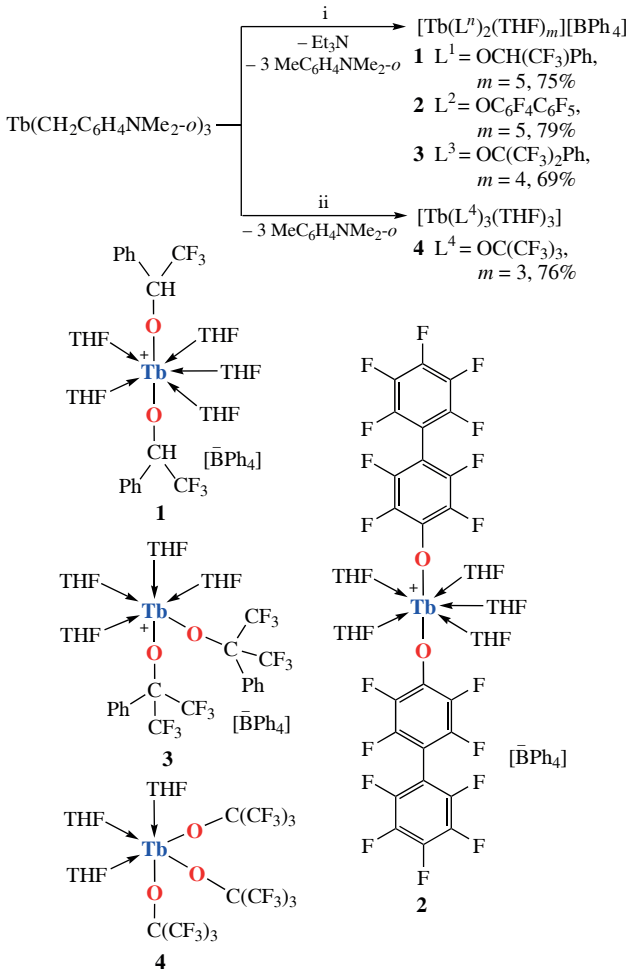

Scheme 1 *Reagents and conditions*: i, (1) $[HNEt_3][BPh_4]$ (1 equiv.), THF, room temperature, (2) L^nH (2 equiv.); ii, L^4H (3 equiv.), THF, room temperature.

The unit cell of compound **1** contains two symmetry-independent cationic mononuclear complexes $\{Tb[OCH(CF_3)Ph]_2(THF)_5\}^+$ **1a**,**b** (Figure 1). In both complexes, the Tb^{3+} ion is in a seven-coordinate environment of two $Ph(CF_3)CHO^-$ ligands located in axial positions and five THF molecules in equatorial positions, which allows it to adopt a slightly distorted pentagonal bipyramidal geometry.

The Tb–O distances to the axial ligands are relatively short, 2.123(2) and 2.126(2) Å in cation **1a** and 2.119(2) Å in the symmetry-independent cation **1b**, whereas the Tb–O distances to the coordinated THF molecules at the equatorial positions are much longer [2.403(2)–2.476(3) Å]. The O–Tb–O axial angle is 177.75(11)° in cation **1a** and 174.07(10)° in cation **1b** (Table S1, see Online Supplementary Materials). The shortest intermolecular Tb···Tb distance is 11.4719(6) Å, indicating that the cationic

† *Crystal data for* **1**–**4**. $C_{60}H_{72}BF_6O_7Tb$ (M = 1188.90) (**1**), $C_{72}H_{68}BF_{18}O_8Tb$ (M = 1572.99) (**2**), $C_{58}H_{62}BF_{12}O_6Tb$ (M = 1252.80) (**3**), $C_{24}H_{24}F_{27}O_6Tb$ (M = 1080.35) (**4**); monoclinic, space group $P2_1/n$ (**1**–**4**), a = 20.4447(4) (**1**), 12.8917(5) (**2**), 20.3100(3) (**3**), 9.7005(2) (**4**), b = 23.0013(4) (**1**), 24.1412(8) (**2**), 13.8765(2) (**3**), 21.5239(6) (**4**) and c = 24.7175(4) (**1**), 23.3340(8) (**2**), 20.6184(3) (**3**), 16.7469(4) (**4**) Å, β = 96.7400(10) (**1**), 92.400(2) (**2**), 111.4950(10) (**3**), 90.2600(10) (**4**)°; V = 11543.2(4) (**1**), 7255.7(4) (**2**), 5406.77(14) (**3**), 3496.59(15) (**4**) Å^3; μ(MoKα) = 12.94 (**1**), 10.73 (**2**), 14 (**3**), 22.5 (**4**) mm^{-1}. Analysis was performed at 100(2) K on a Bruker Quest D8 CMOS diffractometer by standard procedure (graphite monochromated MoKα radiation, ω-scanning). Total of 132510 (**1**), 82936 (**2**), 66630 (**3**), 35492 (**4**) reflections were measured ($4.36 < 2\theta < 65.23°$), 25203 (**1**), 15846 (**2**), 13064 (**3**), 6873 (**4**) unique reflections (R_{int} = 0.0390), 19101 (**1**), 12221 (**2**), 9568 (**3**), 6011 (**4**) reflections with $I > 2\sigma(I)$. The structures were solved and refined using the SHELXTL program package. The structures were defined by direct statistical methods and refined by full-matrix anisotropic approximation for F^2 for all non-hydrogen atoms with SHELXL program. The hydrogen atoms were localized by direct method and refined in the isotropic approximation. GOOF = 1.010 (**1**), 1.023 (**2**), 1.019 (**3**), 1.050 (**4**); final R values: R_1 = 0.0382 (**1**), 0.0426 (**2**), 0.0372 (**3**), 0.1645 (**4**); wR_2 = 0.0768 (**1**), 0.1010 (**2**), 0.0774 (**3**), 0.0652 (**4**) [$I > 2\sigma(I)$]; R_1 = 0.0589 (**1**), 0.0602 (**2**), 0.0594 (**3**), 1.0500 (**4**); wR_2 = 0.0854 (**1**), 0.1106 (**2**), 0.0867 (**3**), 0.0723 (**4**) (all data). Residual electronic density max/min was 0.771/–0.850 (**1**), 0.865/–0.602 (**2**), 1.854/–0.851 (**3**), 1.965/–1.379 (**4**) e Å^{-3}.

CCDC 2206279 (**1**), 2206278 (**2**), 2206277 (**3**) and 2206602 (**4**) contain the supplementary crystallographic data for this paper. These data can be obtained free of charge from The Cambridge Crystallographic Data Centre *via* https://www.ccdc.cam.ac.uk.

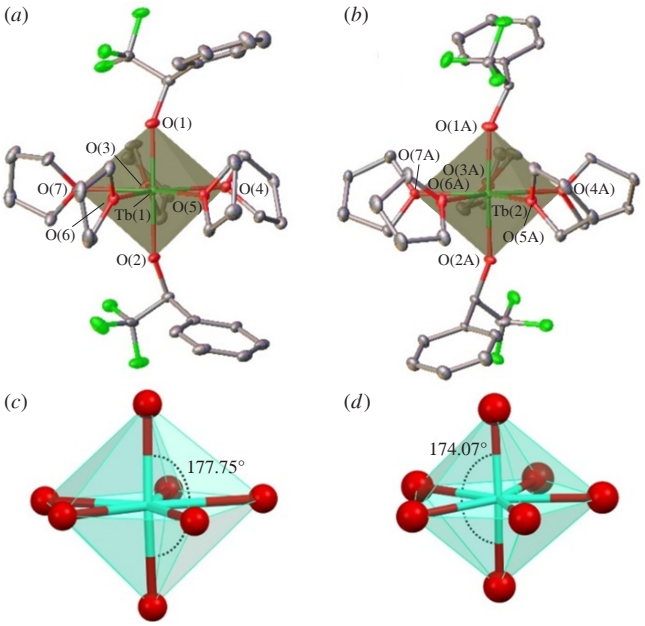

Figure 1 (*a*),(*b*) General view of the coordination environment and (*c*),(*d*) coordination polyhedra of the Tb^{3+} ion in symmetry-independent cationic complexes (*a*),(*c*) **1a** and (*b*),(*d*) **1b**. Hereinafter, hydrogen atoms, minor components of disordered ligands and lattice solvents (where applicable) are omitted for clarity, other atoms are shown as thermal ellipsoids (p = 20%) and only labels of heteroatoms are given.

complexes are relatively well isolated in the crystal. The crystal structure of this compound can be compared with that of a previously published highly luminescent Dy^{3+}-based SMM, $[Dy(OCHMeC_6F_5)_2(THF)_5][BPh_4]$, prepared using the fluorinated $C_6F_5CH(Me)O^-$ ligand. However, the latter presents a slightly distorted octahedral coordination environment of the Dy^{3+} ion, but with a comparable axial angle of 177.5(2)° and comparable short Dy–O distances of 2.101(3) and 2.104(3) Å. In complex **2**, the Tb^{3+} ion in the cationic unit is seven-coordinated by two $C_6F_5C_6F_4O^-$ ligands at axial positions and five THF molecules at equatorial ones (Figure S7, see Online Supplementary Materials). Its coordination polyhedron is a pentagonal bipyramid, but with a more pronounced distortion than in complex **1**, with the O–Tb–O axial angle of 168.64(10)°. Compared to complex **1**, this complex also features longer Tb–O bonds to these ligands [2.160(2) and 2.167(2) Å] and shorter Tb–O bonds to the THF ligands [2.392(3)–2.421(3) Å]. The unit cell of complex **2** (Figure S8) contains four formula units with different orientations. The shortest intermolecular Tb···Tb distance in complex **2** is 12.8917(5) Å, which is larger than in complex **1** due to the bulky $C_6F_5C_6F_4O^-$ ligands. Using the $Ph(CF_3)_2CO^-$ ligand, which is bulkier than $Ph(CF_3)CHO^-$ in complex **1**, affords complex **3** with a Tb^{3+} ion six-coordinated by two $Ph(CF_3)_2CO^-$ ligands and four THF molecules in a distorted octahedral geometry (Figure S9). In this complex, the two $Ph(CF_3)_2CO^-$ ligands are not in axial positions as in complex **1**, but form a *cis* configuration. The O–Tb–O angles are 169.72(8)° and 165.94(9)° between $Ph(CF_3)_2CO^-$ and THF and 164.86(10)° between the two THFs. The Tb–O distances to the $Ph(CF_3)_2CO^-$ ligands are short, 2.117(2) and 2.107(2) Å, while those to the THF molecules range from 2.331(2) to 2.423(2) Å. The crystal packing (see Figure S9) features the shortest intermolecular Tb···Tb distance of 11.2216(7) Å, which is comparable to that in the crystal of complex **1**.

In complex **4**, the Tb^{3+} ion is linked by three $(CF_3)_3CO^-$ ligands and three THF molecules in the *mer* configuration, making it six-coordinated with a distorted octahedral environment (Figure S10). All O–Tb–O angles are comparable and equal to 163.6(2)–165.4(2)°. As expected, the Tb–O distances to the $(CF_3)_3CO^-$ ligands [2.143(6), 2.137(6) and 2.132(6) Å] are shorter than those to the THF molecules [2.411(6)–2.428(6) Å]. Note that the use of relatively small $(CF_3)_3CO^-$ ligand can help reducing the intermolecular Tb···Tb distance to 9.6742(8) Å (see Figure S10).

The temperature-dependent magnetic behavior was investigated in the direct current (dc) mode with an applied magnetic field of 1 kOe. The room temperature χT values of 12.0, 11.7, 11.9 and 11.6 cm^3 K mol^{-1} obtained for complexes **1**–**4**, respectively, are in a relatively good agreement with the value of 11.8 cm^3 K mol^{-1} expected for a single Tb^{3+} ion. The χT values decrease with decreasing temperature, indicating the conventional thermal depopulation of the m_J levels [Figure 2(*a*)]. The field dependence of magnetization curves were obtained at 1.8 K for all compounds. At low fields, the magnetization initially increases significantly, followed by a more gradual rise after 1 kOe. However, magnetization saturation is not reached even at 7 kOe [Figure 2(*b*)]. This behavior indicates a notable magnetic anisotropy, which is commonly observed in lanthanide complexes.

To explore the possibility of slow magnetization relaxation, the dynamic behavior of compounds **1**–**4** at low temperatures in the alternating current (ac) mode was studied. For all compounds, neither the in-phase (χ') nor the out-of-phase (χ'') components of the ac susceptibility show any signals in the absence of a dc magnetic field. For this reason, the frequency dependence of the ac susceptibility was recorded at different applied magnetic fields. However, only compound **1** demonstrated the appearance of χ' and χ'' signals in the applied magnetic field, while compounds **2**–**4** did not show any signals regardless of the magnetic field strength (Figure S11). For this reason, we provide the description of the dynamic behavior only for compound **1**. The χ' and χ'' components for compound **1** show frequency-dependent signals (Figure S12). Figure S13 demonstrates the obtained Cole–Cole figure (χ'' *vs.* χ'), which was fitted using the Debye model. To determine the optimum applied magnetic field at which the relaxation time would be the largest, the field dependence of the relaxation time (Figure S14) was fitted using the equation

$$\tau^{-1} = DH^2T + B_1/(1 + B_2H^2), \quad (1)$$

where the first term describes the direct relaxation for non-Kramers ions and the second defines the QTM. The obtained optimum field of 2 kOe was used for further dynamic measurements to determine the main parameters describing the magnetic relaxation. Figure 3 shows the frequency dependence of the in-phase (χ') and out-of-phase (χ'') components of the ac susceptibility obtained in this optimum dc field. The χ' signal displays a descending portion of the peak, with its ascending portion likely appearing at lower temperatures, while the χ'' component exhibits distinct peaks that shift toward higher frequencies as temperature increases. The corresponding Cole–

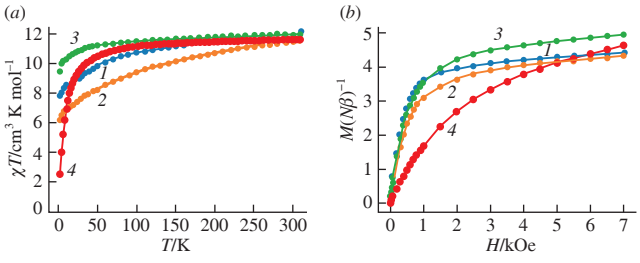

Figure 2 (*a*) Temperature dependences of χT obtained with an applied magnetic field of 1 kOe and (*b*) curves of reduced magnetization [$M(N\beta)^{-1}$] *vs.* magnetic field strength (H) obtained at 1.8 K for complexes (*1*) **1**, (*2*) **2**, (*3*) **3** and (*4*) **4**.

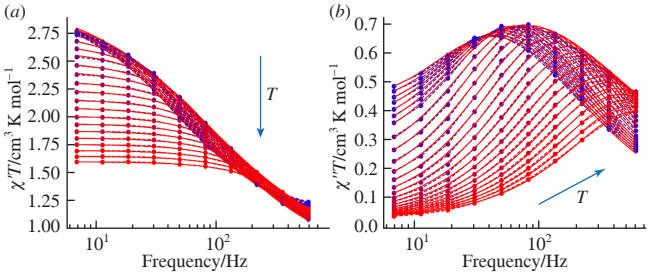

Figure 3 Frequency dependence of (*a*) in-phase (χ') and (*b*) out-of-phase (χ'') components of the ac susceptibility for compound **1** in an applied field of 2 kOe at temperatures from 1.8 to 6 K. The dashed lines are guides for eyes, and the red lines are the result of the Cole–Cole fitting.

Cole plots fitted using the generalized Debye model yielded moderate values of the α parameter (from 0.1 to 0.25), indicating a certain distribution of relaxation times (Figure S15). The temperature dependence of the relaxation time was fitted using the equation

$$\tau^{-1} = DH^2T + \tau_0^{-1}\exp(-\Delta/k_BT), \quad (2)$$

where the first term describes the direct relaxation process for non Kramers-ions and the second one describes the Orbach process (Figure S16). The best fitting parameters obtained are: $\Delta = 12.96 \pm 0.13$ cm^{-1}, $\tau_0 = (1.63 \pm 0.06) \times 10^{-5}$ s and $D = 15.97 \times 0.08$ s^{-1} Oe^{-2} K^{-1}. It should be noted that the use of the equation taking into account the Raman relaxation did not give satisfactory results. This fact suggests that, as expected, the use of a fluorinated ligand in the design of the SMM helps to avoid the presence of Raman relaxation.

The differences in magnetic behavior between compound **1** and compounds **2**–**4** can be explained by several factors, in particular the coordination geometry and ligand structures. Compound **1**, which is a seven-coordinate complex, adopts a slightly distorted pentagonal bipyramidal geometry with a nearly linear O–Tb–O axial angle of 177.7(5)°. This geometry enhances magnetic anisotropy, stabilizing high-spin states and allowing field-induced SMM behavior. The short distances of the Tb–O axial bonds also promote strong axial coordination, which helps align the Tb^{3+} magnetic moment along the applied field, supporting slow relaxation of the magnetization. Although compound **2** is also seven-coordinate, it has less linear O–Tb–O axial angles of 168.64(10)° compared to compound **1**. Compounds **3** and **4** adopt six-coordinate, distorted octahedral geometries. For complex **3**, the axial angle is 169.72(8)°, and for complex **4**, it is 165.4(2)°. These geometries, characterized by more distorted angles and weaker axial coordination, reduce magnetic anisotropy, preventing stabilization of high-spin states and resulting in faster magnetization relaxation.

The solid-state luminescence excitation spectra of compounds **1**–**4** (Figure S17) recorded at 77 K by monitoring the luminescence at 543 nm due to the $^5D_4 \rightarrow {}^7F_5$ transition revealed a large broad band in the 280–370 nm region, which is attributed to the excited states of the ligands. The spectra also contain a series of narrow lines, which can be assigned to the resonant excitation of the Tb^{3+} ion *via* electronic transitions between the $^7F_6$ state and different excited states of Tb^{3+}. Therefore, in all complexes, the excitation of the Tb^{3+} ion emission through the ligand environment can be achieved using radiation in the spectral range of 300–315 nm. Notably, in the excitation spectrum of compound **2**, the intensities of the bands attributed to the Tb^{3+} ion are relatively weak. This can be explained by the fact that the perfluorinated biphenyl moiety apparently functions as an effective antenna for sensitization of Tb^{3+}-centered luminescence.

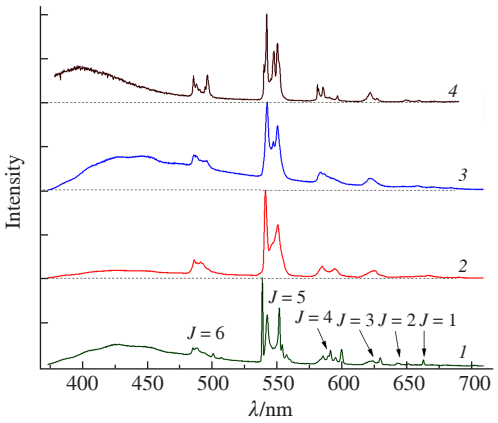

Figure 4 Emission spectra of compounds (*1*) **1**, (*2*) **2**, (*3*) **3** and (*4*) **4** obtained at 77 K upon excitation at 310 nm.

The emission spectra of compounds **1**–**4** upon excitation at 310 nm (Figure 4) displayed characteristic narrow emission bands corresponding to the $^5D_4 \rightarrow {}^7F_J$ ($J = 0$–6) electronic transitions of the Tb^{3+} ion along with a broad band in the blue region of the spectrum attributed to ligand fluorescence. Although the exact excitation maxima varied slightly among the compounds, a consistent excitation wavelength of 310 nm was applied to all samples since minor excitation variations within the UV absorption region of the ligand did not result in noticeable changes in the emission spectra. For compound **2**, the ligand fluorescence is very weak, likely due to efficient ligand-to-Tb^{3+} energy transfer. In contrast, compounds **3** and **4** exhibited prominent ligand-related bands, suggesting less effective energy transfer between the ligands and the Tb^{3+} ion. The Stark structure of the emission bands was better resolved at 77 K than at ambient temperature. Note that compound **3** exhibits near-white emission with the Commission Internationale de l'Éclairage (CIE) 1931 coordinates of (0.25, 0.32).

The photoluminescence decays were recorded with excitation at 310 nm and emission at 543 nm. The initial portion of the decay curve exhibited a fast relaxation component with a characteristic time of about several μs, which could be associated with ligand related fluorescence (Figure S18). The rest of the decay curve can be described by a biexponential relaxation model for all compounds except compound **2**. We attributed the two components to Tb^{3+} emission sites with a slightly different local symmetry of the coordination environment. The characteristic lifetimes (Table S2) for compounds **1**, **3** and **4** were estimated to be remarkably long, up to 1–2 ms. This may be due to the Laporte-forbidden nature of the 4*f*–4*f* transitions in Tb^{3+}, which remain only partially allowed due to slight distortions of the coordination environment, while nonradiative decay channels are effectively suppressed. The overall luminescence quantum yields measured under excitation at 310 nm show moderate values of 2, 11, 6 and 1% for compounds **1**–**4**, respectively.

In conclusion, we synthesized a new series of mononuclear seven- and six-coordinate Tb^{3+} complexes using ligands with different steric bulk. The use of the $Ph(CF_3)CHO^-$ ligand enable the formation of a slightly distorted pentagonal bipyramidal geometry in $\{Tb[OCH(CF_3)Ph]_2(THF)_5\}[BPh_4]$. This complex features the O–Tb–O axial angle of 177.7(5)° with short Tb–O bond distances and represents a remarkable example of luminescent field-induced SMM based on hepta-coordinate Tb^{3+} with an exceptionally long emission lifetime of 1.7 ms. However, the less linearity of the O–Tb–O angle in another seven-coordinate compound **2** leads to the loss of slow magnetization relaxation, while photoluminescence is retained. The six-

coordinate geometry of complexes **3** and **4** is not favorable for the manifestation of magnetic relaxation, but they still exhibit luminescence.

J. L., S. S., G. F., Y. G. thank the University of Montpellier and CNRS for financial support. Authors are grateful to Platform of Analysis and Characterization (PAC) of ICGM for magnetic measurements. The financial support from the Russian Science Foundation is highly acknowledged (project no. 24-13-00275). Single crystal X-ray diffraction data and luminescence excitation spectra and luminescence decays were obtained using the equipment of the Centre for molecular composition studies of INEOS RAS with financial support from the Ministry of Science and Higher Education of the Russian Federation (contract no. 075-00277-24-00).

Online Supplementary Materials

Supplementary data associated with this article can be found in the online version at doi: 10.71267/mencom.7860.

References

1 J. Long, Y. Guari, R. A. S. Ferreira, L. D. Carlos and J. Larionova, *Coord. Chem. Rev.*, 2018, **363**, 57; https://doi.org/10.1016/j.ccr.2018.02.019.
2 J.-H. Jia, Q.-W. Li, Y.-C. Chen, J.-L. Liu and M.-L. Tong, *Coord. Chem. Rev.*, 2019, **378**, 365; https://doi.org/10.1016/j.ccr.2017.11.012.
3 F. Pointillart, O. Cador, B. Le Guennic and L. Ouahab, *Coord. Chem. Rev.*, 2017, **346**, 150; https://doi.org/10.1016/j.ccr.2016.12.017.
4 R. Marin, G. Brunet and M. Murugesu, *Angew. Chem., Int. Ed.*, 2021, **60**, 1728; https://doi.org/10.1002/anie.201910299.
5 E. Bartolomé, A. Arauzo, J. Luzón and L. Gasque, *J. Mater. Chem. C*, 2025, **13**, 831; https://doi.org/10.1039/D4TC03152K.
6 Y. Bi, X.-T. Wang, W. Liao, X. Wang, R. Deng, H. Zhang and S. Gao, *Inorg. Chem.*, 2009, **48**, 11743; https://doi.org/10.1021/ic9017807.
7 J. Larionova, Y. Guari, S. Sene and G. Félix, *Handb. Phys. Chem. Rare Earths*, 2023, **64**, 93; https://doi.org/10.1016/bs.hpcre.2023.10.003.
8 D. A. Gálico, R. Marin, G. Brunet, D. Errulat, E. Hemmer, F. A. Sigoli, J. O. Moilanen and M. Murugesu, *Chem. – Eur. J.*, 2019, **25**, 14625; https://doi.org/10.1002/chem.201902837.
9 E. A. Mikhalyova, M. Zeller, J. P. Jasinski, R. J. Butcher, L. M. Carrella, A. E. Sedykh, K. S. Gavrilenko, S. S. Smola, M. Frasso, S. C. Cazorla, K. Perera, A. Shi, H. G. Ranjbar, C. Smith, A. Deac, Y. Liu, S. M. McGee, V. P. Dotsenko, M. U. Kumke, K. Müller-Buschbaum, E. Rentschler, A. W. Addison and V. V. Pavlishchuk, *Dalton Trans.*, 2020, **49**, 7774; https://doi.org/10.1039/D0DT00600A.
10 S. Shintoyo, K. Murakami, T. Fujinami, N. Matsumoto, N. Mochida, T. Ishida, Y. Sunatsuki, M. Watanabe, M. Tsuchimoto, J. Mrozinski, C. Coletti and N. Re, *Inorg. Chem.*, 2014, **53**, 10359; https://doi.org/10.1021/ic501453h.
11 K. Ehama, Y. Ohmichi, S. Sakamoto, T. Fujinami, N. Matsumoto, N. Mochida, T. Ishida, Y. Sunatsuki, M. Tsuchimoto and N. Re, *Inorg. Chem.*, 2013, **52**, 12828; https://doi.org/10.1021/ic4022273.
12 S. Yamauchi, T. Fujinami, N. Matsumoto, N. Mochida, T. Ishida, Y. Sunatsuki, M. Watanabe, M. Tsuchimoto, C. Coletti and N. Re, *Inorg. Chem.*, 2014, **53**, 5961; https://doi.org/10.1021/ic5001599.
13 L. E. do N. Aquino, G. A. Barbosa, J. de L. Ramos, S. O. K. Giese, F. S. Santana, D. L. Hughes, G. G. Nunes, L. Fu, M. Fang, G. Poneti, A. N. Carneiro Neto, R. T. Moura, Jr., R. A. S. Ferreira, L. D. Carlos, A. G. Macedo and J. F. Soares, *Inorg. Chem.*, 2021, **60**, 892; https://doi.org/10.1021/acs.inorgchem.0c03020.
14 D. M. Lyubov, A. V. Cherkasov and A. A. Trifonov, *Mendeleev Commun.*, 2024, **34**, 43; https://doi.org/10.1016/j.mencom.2024.01.013.
15 P. P. Ferreira da Rosa, Y. Kitagawa and Y. Hasegawa, *Coord. Chem. Rev.*, 2020, **406**, 213153; https://doi.org/10.1016/j.ccr.2019.213153.
16 P. Kalita, J. Acharya and V. Chandrasekhar, *J. Magn. Magn. Mater.*, 2020, **498**, 166098; https://doi.org/10.1016/j.jmmm.2019.166098.
17 F. Gao, L. Cui, W. Liu, L. Hu, Y.-W. Zhong, Y.-Z. Li and J.-L. Zuo, *Inorg. Chem.*, 2013, **52**, 11164; https://doi.org/10.1021/ic401421h.
18 K. Yanagisawa, T. Nakanishi, Y. Kitagawa, T. Seki, T. Akama, M. Kobayashi, T. Taketsugu, H. Ito, K. Fushimi and Y. Hasegawa, *Eur. J. Inorg. Chem.*, 2015, 4769; https://doi.org/10.1002/ejic.201500820.
19 J.-L. Liu, Y.-C. Chen, Y.-Z. Zheng, W.-Q. Lin, L. Ungur, W. Wernsdorfer, L. F. Chibotaru and M.-L. Tong, *Chem. Sci.*, 2013, **4**, 3310; https://doi.org/10.1039/c3sc50843a.
20 J. Long, A. O. Tolpygin, D. M. Lyubov, N. Yu. Rad'kova, A. V. Cherkasov, Y. V. Nelyubina, Y. Guari, J. Larionova and A. A. Trifonov, *Dalton Trans.*, 2021, **50**, 8487; https://doi.org/10.1039/D1DT01319J.
21 A. N. Selikhov, G. Félix, D. M. Lyubov, Y. V. Nelyubina, A. V. Cherkasov, S. Sene, I. V. Taydakov, M. T. Metlin, A. A. Tyutyunov, Y. Guari, J. Larionova and A. A. Trifonov, *Dalton Trans.*, 2024, **53**, 6352; https://doi.org/10.1039/D3DT04375D.
22 J. Long, D. M. Lyubov, A. A. Kissel', I. A. Gogolev, A. A. Tyutyunov, Y. V. Nelyubina, F. Salles, Y. Guari, A. V. Cherkasov, J. Larionova and A. A. Trifonov, *CrystEngComm*, 2022, **24**, 6953; https://doi.org/10.1039/d2ce00856d.
23 Y. Ma, Y.-Q. Zhai, Q.-C. Luo, Y.-S. Ding and Y.-Z. Zheng, *Angew. Chem., Int. Ed.*, 2022, **61**, e202206022; https://doi.org/10.1002/anie.202206022.
24 D. M. Lyubov and A. A. Trifonov, *Russ. Chem. Bull.*, 2024, **73**, 1497; https://doi.org/10.1007/s11172-024-4271-1.
25 S. Harder, *Organometallics*, 2005, **24**, 373; https://doi.org/10.1021/om049327p.
26 S. Harder, C. Ruspic, N. N. Bhriain, F. Berkermann and M. Schürmann, *Z. Naturforsch., B: J. Chem. Sci.*, 2008, **63**, 267; https://doi.org/10.1515/znb-2008-0307.

Received: 27th June 2025; Com. 25/7860